Magnetic structure and exchange interactions of the van der Waals CrPS$_4$ monolayer under strain: A first-principles study

Xiangyan Bo ,[1] Feng Li,[1] Xiaomiao Yin ,[1] Yu Chen ,[1] Xiangang Wan,[2,3] and Yong Pu[1,*]

[1]*New Energy Technology Engineering Laboratory of Jiangsu Province & School of Science,*
Nanjing University of Posts and Telecommunications, Nanjing 210023, China
[2]*National Laboratory of Solid State Microstructures and School of Physics, Nanjing University, Nanjing 210093, China*
[3]*Collaborative Innovation Center of Advanced Microstructures, Nanjing University, Nanjing 210093, China*

Intrinsic van der Waals layered magnets have attracted much attention. Herein, we carry out a comprehensive investigation of the air-stable two-dimensional van der Waals semiconducting magnet CrPS$_4$ using first-principles calculations. With the first-principles linear response method and Monte Carlo simulations, we estimate the magnetic exchange constants and magnetic transition temperatures of both bulk and monolayer CrPS$_4$. We find that the main intralayer interactions of bulk CrPS$_4$ are all ferromagnetic coupling, while the dominant interlayer interactions of bulk CrPS$_4$ are antiferromagnetic coupling. Using the calculated magnetic exchange constants, our Monte Carlo simulations show that monolayer CrPS$_4$ has Curie temperature $T_C = 34$ K. Moreover, we study the effect of uniaxial strain of monolayer CrPS$_4$, and find that a uniaxial compressive strain greater than 6% along the *b* axis would cause the magnetic ground state to change into an up-up-down-down magnetic order along the *b* axis.

I. INTRODUCTION

The search for two-dimensional (2D) materials with novel properties has been driven by continuous development of modern device applications. Since the recent discoveries of antiferromagnetism in FePS$_3$ [1] and ferromagnetism in CrI$_3$ [2], Cr$_2$Ge$_2$Te$_6$ [3], and Fe$_3$GeTe$_2$ [4], 2D magnetic materials have attracted great attention due to their novel physical properties and potential applications in spintronics. The ideal candidates for 2D magnetic materials are layered van der Waals materials, which are readily cleavable due to the weak interactions between the layers [5]. Therefore, a large number of 2D magnetic materials are predicted, such as transition metal halides (MX$_3$/MX$_2$, X = Cl/Br/I) [6–9], transition metal dichalcogenides (MX$_2$, X = O/S/Se/Te) [10–12], ternary transition metal compounds (ABX$_3$) [13–17], etc. Although there is a wide variety of potential 2D magnets from theoretical predictions, making these ultrathin 2D magnets in a laboratory is difficult [18]. Thus, it is still very important to carry out more in-depth theoretical research on the magnetic exchange mechanisms of 2D magnetic systems.

CrPS$_4$ is a layered van der Waals magnet, which has already been exfoliated into monolayers [19]. Recently, monolayer CrPS$_4$ has been reported to show excellent stability in air [20]. Absorption and photoluminescence measurements indicate that CrPS$_4$ is a semiconductor with an electronic gap of 1.31 eV [19]. However, despite many experimental and theoretical investigations, [21–25] have shown that CrPS$_4$ crystal is antiferromagnetic (AFM), the magnetic ground state

of CrPS$_4$ is still under debate. Pei *et al*. [21] proposed C-type AFM as the ground state, however, data from recent experiments [20,24,25] suggest an A-type AFM magnetic ground state with intralayer ferromagnetic (FM) and interlayer AFM. In addition, two density functional theory (DFT) calculations suggested an A-type AFM [22] and an X-type AFM [23], respectively. In contrast to the extensive studies of magnetic structures [20–27], magnetic exchange interactions have received much less attention [20,23,24,28]. Moreover, most theoretical studies [23,28] assume the nearest neighbor interaction $J_1 = J_2$. However, this simplified model cannot reproduce the neutron-scattering experiment results well [24]. Therefore, accurate prediction of magnetic properties requires a detailed knowledge of the magnetic exchange Hamiltonian, and the calculation of exact magnetic exchange constants of CrPS$_4$ is still an interesting issue and the focus of our current work.

In this work, based on first-principles calculations, we systematically study the electronic and magnetic properties of both bulk and monolayer CrPS$_4$. Our calculations show that bulk (monolayer) CrPS$_4$ is an insulator with a band gap of 1.22 eV (1.35 eV). Using the first-principles linear response (FPLR) method [29,30], we calculate the magnetic exchange constants. We find that the main intralayer interactions of both bulk and monolayer CrPS$_4$ are all FM coupling, while the dominant interlayer interactions of bulk CrPS$_4$ are AFM coupling. Based on the obtained magnetic exchange interactions, the magnetic transition temperatures are estimated by Monte Carlo simulations. In addition, we study the effect of uniaxial strain on the exchange interactions of monolayer CrPS$_4$, and find that a uniaxial compressive strain along the *b* axis would cause the magnetic ground state to change into an up-up-down-down magnetic order along the *b* axis.

*Corresponding author: puyong@njupt.edu.cn

II. METHOD

The electronic band structure calculations have been carried out by using the full potential linearized augmented plane wave method as implemented in the WIEN2K package [31]. For the exchange-correlation potential, the generalized gradient approximation (GGA) is used. To better take into account the interlayer van der Waals forces of bulk $CrPS_4$, we also perform calculations adopting a nonlocal van der Waals density functional in the form of optB88-vdW [32,33]. Based on the experimental lattice constants $a = 10.85$ Å, $b = 7.25$ Å, and $c = 6.10$ Å [24], we optimize the internal atomic coordinate for bulk $CrPS_4$. The crystal structure of monolayer $CrPS_4$ is fully optimized, while the vacuum space is set to be 15 Å to avoid interactions with other neighboring layers. The phonon spectrum is calculated by using the PHONOPY code [34]. GGA+U calculations are also performed for including the effect of Coulomb repulsion in the Cr-$3d$ orbital [35]. We also test various values of U and J, and find that our main conclusions do not depend on the parameters ($U = 2 - 4$ eV and $J = 0 - 1$ eV). Here, we use the values of $U = 4$ eV and $J = 1$ eV, which can reproduce the experimental magnetic moments and band gap very well [19,24,25,27]. The basic functions were expanded to $R_{mt} \times K_{max} = 7$, where R_{mt} is the smallest of the muffin-tin sphere radii and K_{max} is the largest reciprocal lattice vector used in the plane-wave expansion. The $10 \times 10 \times 10$, $10 \times 10 \times 5$, and $10 \times 10 \times 1$ k-point meshes are used for the primitive cell, super cell, and slab calculations, respectively. The self-consistent calculations are considered to be converged when the difference in the total energy of the crystal does not exceed 0.01 mRy at consecutive steps.

The exchange constants J's are the basis for helping us understand the magnetic properties. Here, we use the FPLR method to calculate the exchange interactions, which is based on a combination of the magnetic force theorem [29] and the linear response method [30]. The exchange interaction constant is determined by the calculation of the second variation of total energy with a small deviation of the magnetic moment [30]. This method directly computes the lattice Fourier transform $J(q)$ of the exchange interaction $J(R_l)$, so it is easy to calculate the exact long-range exchange interactions. Recently, this technique has been successfully used to evaluate magnetic interactions in a variety of materials [29,30,36–44]. Based on the calculated magnetic exchange interactions, we explore the magnetic phase diagrams by a replica-exchange Monte Carlo method [45].

III. RESULTS AND DISCUSSION

A. Bulk CrPS$_4$

The crystal structure of bulk $CrPS_4$ belongs to space group C_2 (No. 5). There are four independent lattice constants: $a = 10.85$ Å, $b = 7.25$ Å, $c = 6.10$ Å, and $\beta = 92°$ [24]. There are two Cr atoms in each primitive cell. As shown in Fig. 1, the Cr atom is surrounded by six S atoms, forming a distorted octahedra. CrS_6 octahedra are connected by S-S edge-sharing along the b axis to form a one-dimensional chain, and then bridged by P atoms along the a axis to form the 2D lattice. The
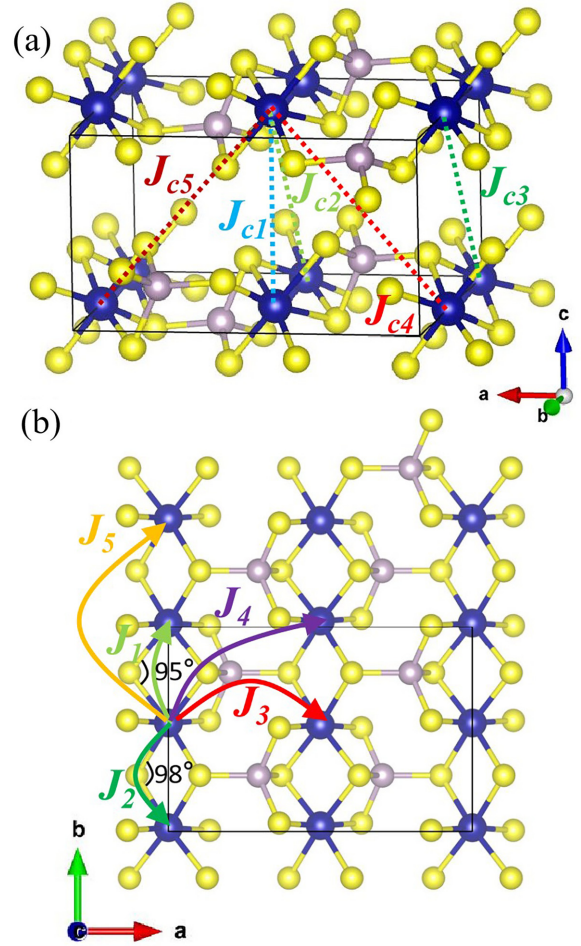

FIG. 1. Definitions of the magnetic exchange interactions. (a) The bulk crystal structure of $CrPS_4$. (b) Top view of the monolayer $CrPS_4$. The blue, light gray, and yellow balls represent the Cr, P, and S ions, respectively.

vertical stacking of each monolayer in bulk $CrPS_4$ is along the c axis, where the angle between the a and c axes is $\beta = 92°$.

Based on the crystal structure suggested by the experiment, we perform the first-principles calculations. Since different magnetic ground states have been proposed from experiments and DFT calculations, here we first perform the GGA+U calculations based on FM configuration. The calculated band gap is 1.14 eV, which is smaller than the experimental results (1.31 eV) [19]. The nominal valence of S is -2, while that of P is $+5$. Hence, the nominal valence of Cr is $+3$. The calculated magnetic moment on the Cr atom is 2.83 μ_B, consistent with the high spin state of $S = 3/2$ and the experimental value of 2.8 μ_B [24].

To determine the magnetic structure in bulk $CrPS_4$, we use the FPLR method to calculate exchange interactions. As shown in Fig. 1, we depict the main magnetic interactions. Based on the calculated FM structure, we estimate and give the magnetic exchange constants with bond lengths less than 8.5 Å in Table I. Among them, J_1 and J_2 dominate over the others in strength, which determines the FM order along the b axis. Since both J_3 and J_4 are FM interactions, this suggests that $CrPS_4$ is FM in the ab layer. On the other hand, the

TABLE I. Calculated magnetic exchange constants (in meV) for the two magnetic configurations of bulk $CrPS_4$ evaluated from the GGA+U scheme. The Cr-Cr distances and the corresponding number of neighbors are presented in the second and third columns.

	Distance (Å)	NN	FM	A-AFM
J_1	3.564	1	−3.41	−3.41
J_2	3.691	1	−3.80	−3.80
J_3	5.425	2	−0.186	−0.186
J_4	6.526	4	−0.360	−0.360
J_5	7.256	2	0.275	0.275
J_{c1}	6.105	2	−0.016	−0.015
J_{c2}	7.070	2	0.022	0.022
J_{c3}	7.135	2	0.024	0.025
J_{c4}	8.022	2	0.003	0.002
J_{c5}	8.311	2	0.067	0.065

interlayer first-nearest-neighbor interaction $J_{c1} = -0.016$ meV, seems to imply that the spins of the top and bottom monolayers should have the same directions. However, the slightly distant interlayer interactions J_{c2}, J_{c3}, and J_{c5} are AFM interactions, and even stronger than J_{c1}. Overall the magnetic ground state calculated from the Heisenberg model is A-type AFM, which is consistent with the recent experimental results [20,24,25].

Based on the ground state magnetic structure determined above, the band structures and the density of states (DOS) from GGA+U calculations are presented in Figs. 2(a) and 3(a). Our calculations show that $CrPS_4$ is an insulator with a band gap of 1.22 eV, which is in good agreement with the experimental results (1.31 eV) [19]. From the DOS results, we find that the conduction bands lying in 2–4 eV are mainly composed by the Cr-3d states, while the topmost valence bands within 2 eV below the Fermi level arise mainly from the S-3p states. The calculated magnetic moment on the Cr atom is 2.83 μ_B, which is the same as the magnetic moment

calculated by FM order. This indicates that the magnetism in $CrPS_4$ is quite localized. Moreover, the total energy of the A-type AFM is about 2.2 meV/f.u. lower than that of the FM state by the direct total energy calculations, confirming the ground state from the calculated magnetic interactions.

Using the FPLR method, we also calculate and give the exchange interactions for A-type AFM structure in Table I. We find that the values of exchange constants with different magnetic configurations are almost the same. For $CrPS_4$, a common route to simplify the analysis is to introduce the constraint $J_1 = J_2$ [20,23,28], although they are not equivalent. It is speculated that J_1 should have stronger FM interaction according to the Goodenough-Kanamori-Anderson rules [46–48], as the Cr-S-Cr bond angle of J_1 is closer to 90° than that of J_2. However, we note that in addition to the Cr-S-Cr bond, the exchange channel of J_1 can also be realized by the Cr-S-P-S-Cr chain, so the relative strength of the exchange interactions J_1 and J_2 cannot be simply determined. In this case, our calculations show that J_1 (−3.41 meV) is weaker than J_2 (−3.80 meV). Our J_1 and J_2 are slightly larger than the fitting results ($J_1 = -2.09$ meV and $J_2 = -2.96$ meV) of the neutron-scattering measurements [24]. The sum of J_3 and J_4 (−0.546 meV) is very close to the fitting exchange interaction (−0.51 meV) along the a axis, while the sum of J_{c1}, J_{c2}, J_{c3}, J_{c4}, and J_{c5} (0.099 meV) is smaller than the fitting interlayer interaction (0.16 meV) along the c axis [24].

Based on the calculated magnetic exchange constants, we use the following Heisenberg model and carry out Monte Carlo simulations to estimate the magnetic transition temperature for $CrPS_4$:

$$H = \sum_{i<j} J_{ij} S_i \cdot S_j - \sum_i A (S_i^z)^2, \qquad (1)$$

where A is the magnetic anisotropy energy (MAE). The full spin ($S = 3/2$) is included in this model. We adopt $L \times L \times L$ supercells with $L = 8 - 14$ in our Monte Carlo simulations.
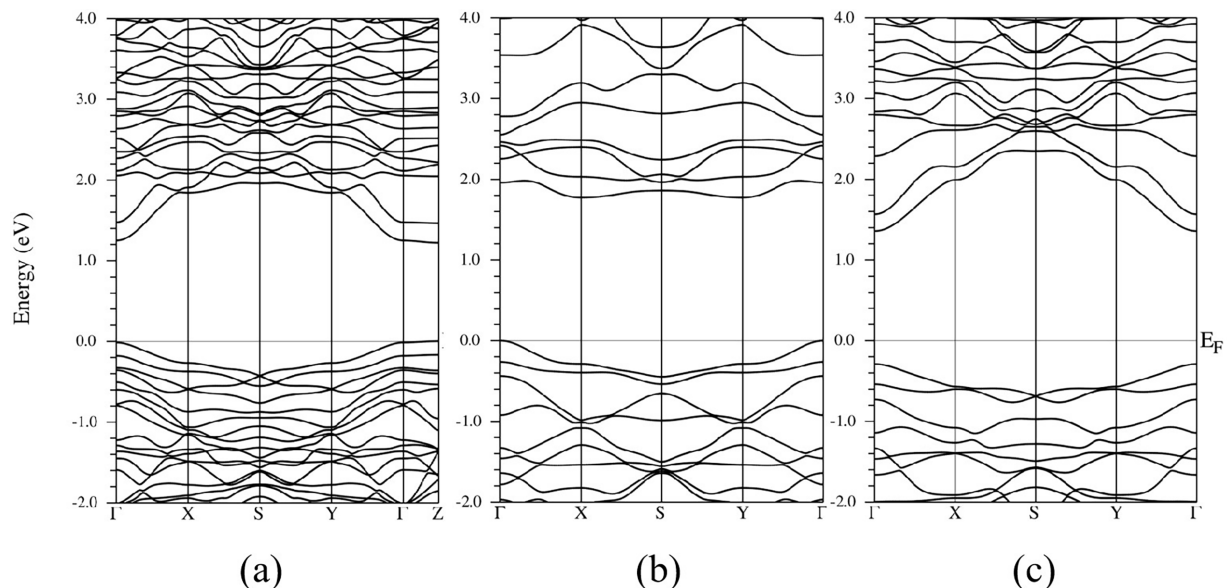

FIG. 2. Band structures of $CrPS_4$. (a) GGA+U calculation in the AFM ground state for bulk $CrPS_4$. (b), (c) Spin-up and spin-down channel, respectively, from GGA+U calculation for monolayer $CrPS_4$. The Fermi energy is set to zero.
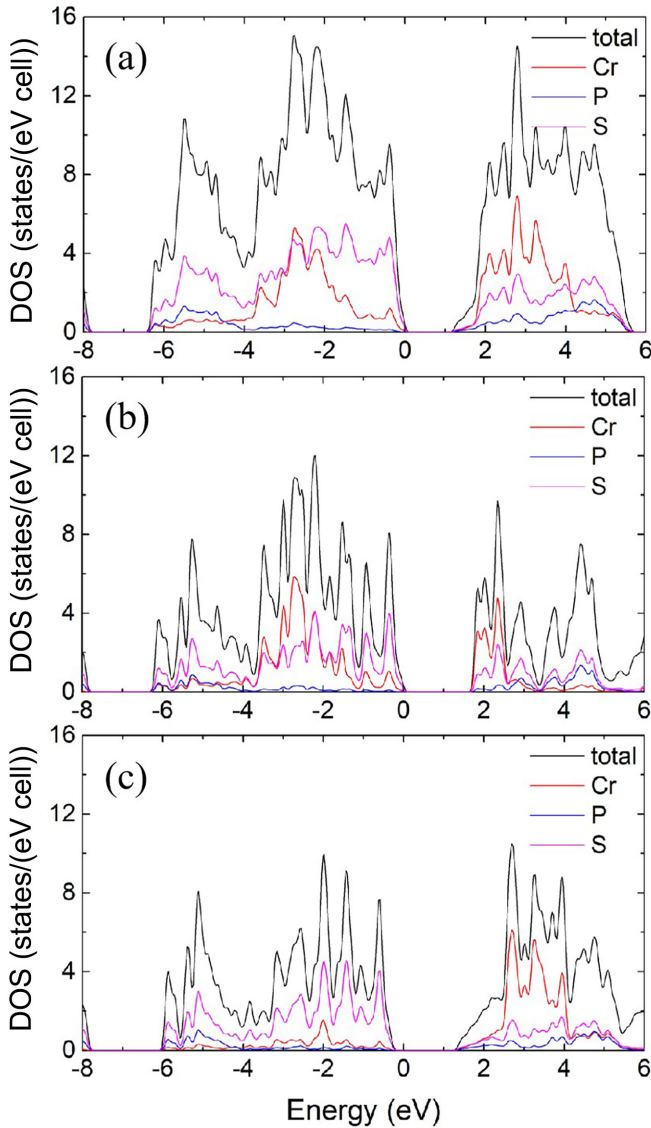
FIG. 3. DOS of $CrPS_4$. (a) GGA+U calculation in the AFM ground state for bulk $CrPS_4$. (b), (c) Spin-up and spin-down channel, respectively, from GGA+U calculation for monolayer $CrPS_4$. The Fermi energy is set to zero.

For $CrPS_4$, various experiments show that the MAE ranges from 0.0042 to 0.0058 meV [20,24]. To avoid ambiguity, we use MAE as a constant in the simulations below. The calculated magnetic transition temperature with $L = 12$ is around 35 K, which excellently agrees with the experimental value of 36–38 K [19,21,25,27,49].

B. Monolayer $CrPS_4$

The monolayer $CrPS_4$ is phasestable and can maintain the FM order in air for more than one day [20]. Based on the optimized structure ($a = 10.87$ Å and $b = 7.34$ Å), the phonon dispersions of monolayer $CrPS_4$ along high symmetry lines are calculated by using the PHONOPY code. As shown in Fig. 4, there are no imaginary frequencies in phonon dispersions, suggesting that the structure of monolayer $CrPS_4$ is dynamically stable. We perform GGA+U calculations for
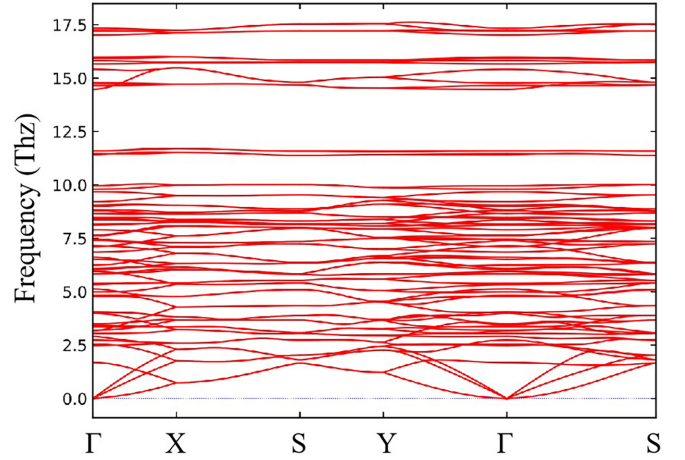

FIG. 4. Calculated phonon dispersions of monolayer $CrPS_4$.

monolayer $CrPS_4$ and give the band structures and DOS in Figs. 2(b) and 2(c) and Figs. 3(b) and 3(c). The S = 3/2 state is confirmed as the spin-down orbital if Cr is completely empty. The calculated magnetic moment of the Cr ion is 2.86 μ_B. Our calculations show that monolayer $CrPS_4$ is an insulator with a band gap of 1.35 eV, slightly larger than that of bulk $CrPS_4$.

Similarly, the magnetic exchange interactions of monolayer $CrPS_4$ are also calculated using FPLR method, as displayed in Table II. We find that the sign of exchange constant in monolayer $CrPS_4$ is the same as that in bulk $CrPS_4$, which means that monolayer $CrPS_4$ is FM ordered. The J_1 (−3.88 meV) of monolayer $CrPS_4$ is stronger than that (−3.41 meV) in bulk $CrPS_4$, while J_2 (−3.54 meV) of monolayer $CrPS_4$ is weaker than that (−3.80 meV) in bulk $CrPS_4$. In contrast to the case of bulk $CrPS_4$, J_1 (−3.88 meV) of monolayer $CrPS_4$ is stronger than J_2 (−3.54 meV). The J_3 (−0.238 meV) and J_4 (−0.373 meV) in monolayer $CrPS_4$ are stronger than those ($J_3 = −0.186$ meV and $J_4 = −0.360$ meV) in bulk $CrPS_4$.

With the calculated magnetic exchange constants, we also simulate the magnetic phase diagram of the monolayer $CrPS_4$. Figure 5 depicts the magnetization and magnetic susceptibility as functions of temperature for a 40×40 lattice. Same as the bulk case, the MAE is set to 0.005 meV. The calculated magnetic transition temperature (34 K) is slightly lower than that of bulk $CrPS_4$ (35 K), which is consistent with the experimental results [20].

TABLE II. Calculated magnetic exchange constants (in meV) of monolayer $CrPS_4$ evaluated from the GGA+U scheme. The Cr-Cr distances and the corresponding number of neighbors are presented in the second and third columns.

	Distance (Å)	NN	This work
J_1	3.608	1	−3.88
J_2	3.737	1	−3.54
J_3	5.436	2	−0.238
J_4	6.560	4	−0.373
J_5	7.345	2	0.215
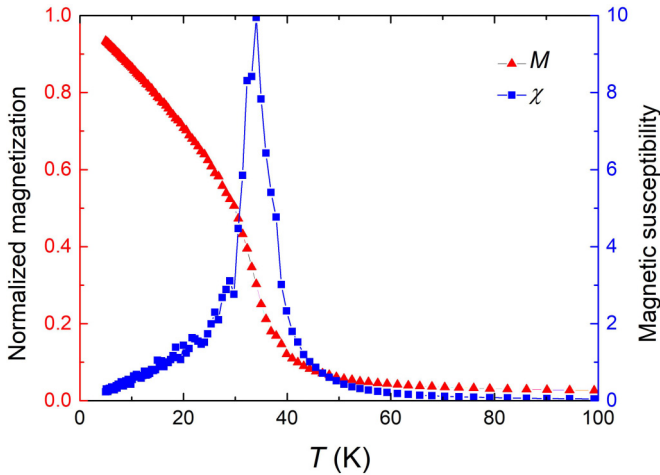
FIG. 5. Monte Carlo simulations of the magnetization and magnetic susceptibility for the CrPS$_4$ monolayer.

FIG. 7. The exchange constants for monolayer CrPS$_4$ under a uniaxial strain along the (a) a or (b) b axis.

C. Strain effect

We investigate the stability of ferromagnetism for monolayer CrPS$_4$ with a uniaxial strain along the a or b axis. In order to understand whether FM coupling can be achieved experimentally, we consider a possible structural breakage in the considered range of strain. Figures 6(a) and 6(b) show the variation of strain energy with applied strain, which is a quadratic function of strain. This indicates that monolayer CrPS$_4$ can withstand 10% uniaxial strain. As shown in Figs. 6(c)–6(f), we find that the strain along the a axis has
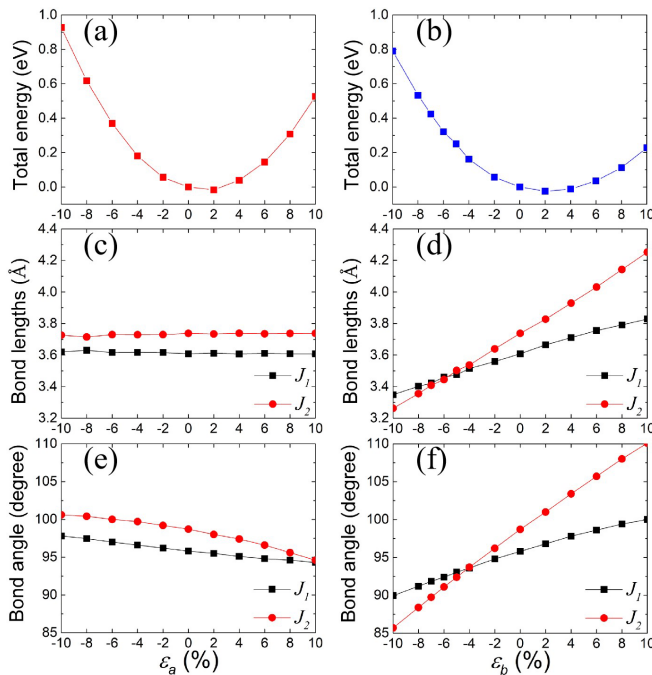

FIG. 6. The total energy of FM state for monolayer CrPS$_4$ under a uniaxial strain along the (a) a and (b) b axis. The bond lengths of J_1 and J_2 under a uniaxial strain along the (c) a and (d) b axis. The bond angles of J_1 and J_2 under a uniaxial strain along the (e) a and (f) b axis.
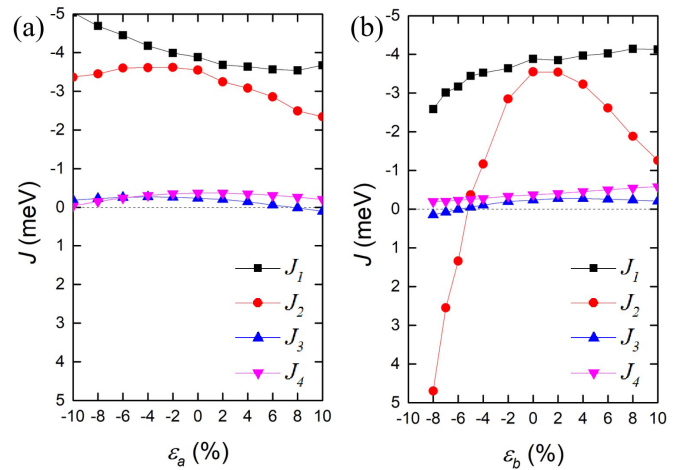
little effect on the bond lengths and angles of J_1 and J_2, while the effect of strain along the b axis on J_2 is very different from that on J_1. Because the P atom is closer to the Cr-Cr bond corresponding to J_1, J_1 is less affected by the strain. However, the uniaxial strain along the b axis has a great influence on the bond length and angle of J_2. When the level of compressive strain along the b axis reaches 6%, the bond length of J_2 (3.44 Å) is smaller than that of J_1 (3.46 Å), and the bond angle of J_2 (91°) is also smaller than that of J_1 (92°).

The magnetic ground state of monolayer CrPS$_4$ is governed not only by the superexchange interaction but also by the direct exchange interaction. As mentioned above, the superexchange with a bond angle approaching 90° gives a FM coupling. On the other hand, for the direct exchange interaction, the direct overlap of d orbitals on adjacent Cr atoms leads to AFM coupling, which is determined by the distance between adjacent Cr atoms. Therefore, it can be expected that when the Cr-Cr distance is short, the total interaction is AFM, while the increase of the Cr-Cr distance favors the FM interaction.

We also calculate the exchange interactions under uniaxial strain using the FPLR method, and simulate the transition temperatures on a 40×40 lattice by using the Monte Carlo method. The exchange constants and magnetic transition temperature as the function of the uniaxial strain level are shown in Figs. 7 and 8. We find that J_1 is moderately enhanced by a compressive strain along the a axis or a tensile strain along the b axis, but J_2 is strongly reduced by a compressive strain or a tensile strain along the b axis. When the compressive strain along the b axis is applied to monolayer CrPS$_4$, the Cr-Cr bond length of J_2 rapidly decreases with the increase of the strain, as shown in Fig. 6(d). Therefore, the AFM direct exchange interaction is gradually enhanced, and when the level of compressive strain along the b axis reaches 6%, J_2 changes from FM to AFM, as shown in Fig. 7(b). Since the dominant magnetic interaction J_1 is FM and J_2 is AFM, the result is that the magnetic ground state is an up-up-down-down magnetic order along the b axis. In addition, J_3 is reduced by a tensile strain along the a axis or compressive strain along the b axis, and J_4 is enhanced by a tensile strain along the b axis. While
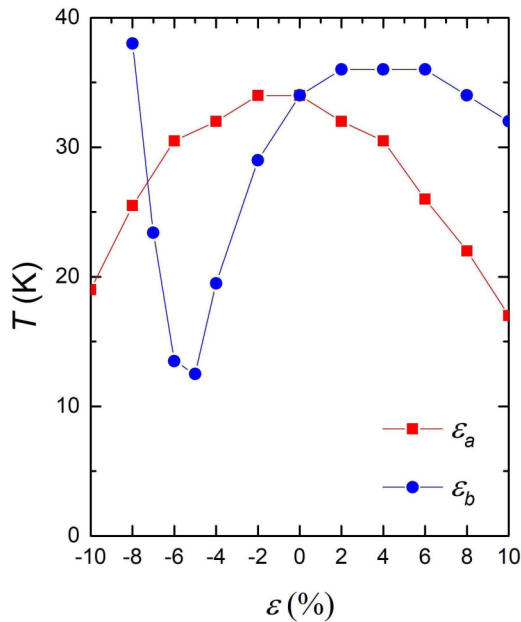
FIG. 8. The magnetic transition temperature of monolayer CrPS$_4$ under a uniaxial strain along the a or b axis.

reveal that the bulk (monolayer) CrPS$_4$ is an insulator with a band gap of 1.22 eV (1.35 eV). Calculations of the magnetic exchange constants using the first-principles linear response method reveal that the magnetic ground state of bulk CrPS$_4$ is A-type AFM. The reason for the relationship between the strength of dominant magnetic interactions J_1 and J_2 is discussed. Moreover, the strain effect for monolayer CrPS$_4$ is demonstrated. The uniaxial strain along the b axis significantly affects the Cr-Cr bond and interaction strength of J_2. When the level of compressive strain along the b axis is greater than 6%, J_2 changes from FM to AFM, resulting in the up-up-down-down magnetic order along the b axis. This work demonstrate accurate calculations of magnetic exchange constants for CrPS$_4$ materials, which will help to deeply understand their electronic and magnetic properties and support further study of them.

the level of tensile strain along the b axis reaches 4%, T_C of monolayer CrPS$_4$ increases from 34 K to 36 K. If we further increase the tensile strain level, the T_C will decrease.

IV. CONCLUSIONS

In conclusion, a systematic investigation of CrPS$_4$ using first-principles calculations is demonstrated. Our calculations

[1] J.-U. Lee, S. Lee, J. H. Ryoo, S. Kang, T. Y. Kim, P. Kim, C.-H. Park, J.-G. Park, and H. Cheong, Ising-type magnetic ordering in atomically thin FePS$_3$, Nano Lett. **16**, 7433 (2016).

[2] B. Huang, G. Clark, E. Navarro-Moratalla, D. R. Klein, R. Cheng, K. L. Seyler, D. Zhong, E. Schmidgall, M. A. McGuire, D. H. Cobden, W. Yao, D. Xiao, P. Jarillo-Herrero, and X. Xu, Layer-dependent ferromagnetism in a van der Waals crystal down to the monolayer limit, Nature (London) **546**, 270 (2017).

[3] C. Gong, L. Li, Z. Li, H. Ji, A. Stern, Y. Xia, T. Cao, W. Bao, C. Wang, Y. Wang, Z. Q. Qiu, R. J. Cava, S. G. Louie, J. Xia, and X. Zhang, Discovery of intrinsic ferromagnetism in two-dimensional van der Waals crystals, Nature (London) **546**, 265 (2017).

[4] Y. Deng, Y. Yu, Y. Song, J. Zhang, N. Z. Wang, Z. Sun, Y. Yi, Y. Z. Wu, S. Wu, J. Zhu, J. Wang, X. H. Chen, and Y. Zhang, Gate-tunable room-temperature ferromagnetism in two-dimensional Fe$_3$GeTe$_2$, Nature (London) **563**, 94 (2018).

[5] G. R. Bhimanapati, Z. Lin, V. Meunier, Y. Jung, J. Cha, S. Das, D. Xiao, Y. Son, M. S. Strano, V. R. Cooper, L. Liang, S. G. Louie, E. Ringe, W. Zhou, S. S. Kim, R. R. Naik, B. G. Sumpter, H. Terrones, F. Xia, Y. Wang *et al.*, Recent advances in two-dimensional materials beyond graphene, ACS Nano **9**, 11509 (2015).

[6] V. V. Kulish and W. Huang, Single-layer metal halides MX$_2$ (X = Cl, Br, I): Stability and tunable magnetism from first principles and Monte Carlo simulations, J. Mater. Chem. C **5**, 8734 (2017).

[7] S. Tomar, B. Ghosh, S. Mardanya, P. Rastogi, B. S. Bhadoria, Y. S. Chauhan, A. Agarwal, and S. Bhowmick, Intrinsic magnetism in monolayer transition metal trihalides: A comparative study, J. Magn. Magn. Mater. **489**, 165384 (2019).

[8] A. S. Botana and M. R. Norman, Electronic structure and magnetism of transition metal dihalides: Bulk to monolayer, Phys. Rev. Mater. **3**, 044001 (2019).

[9] Z.-X. Shen, C. Su, and L. He, High-throughput computation and structure prototype analysis for two-dimensional ferromagnetic materials, npj Comput. Mater. **8**, 132 (2022).

[10] Z. Sun, H. Lv, Z. Zhuo, A. Jalil, W. Zhang, X. Wu, and J. Yang, A new phase of the two-dimensional ReS$_2$ sheet with tunable magnetism, J. Mater. Chem. C **6**, 1248 (2018).

[11] H. van Gog, W.-F. Li, C. Fang, R. S. Koster, M. Dijkstra, and M. van Huis, Thermal stability and electronic and magnetic properties of atomically thin 2D transition metal oxides, npj 2D Mater. Appl. **3**, 18 (2019).

[12] L. Liu, S. Chen, Z. Lin, and X. Zhang, A Symmetry-Breaking Phase in Two-Dimensional FeTe$_2$ with Ferromagnetism

above Room Temperature, J. Phys. Chem. Lett. **11**, 7893 (2020).

[13] M. Yu, X. Liu, and W. Guo, Novel two-dimensional ferromagnetic semiconductors: Ga-based transition-metal trichalcogenide monolayers, Phys. Chem. Chem. Phys. **20**, 6374 (2018).

[14] X.-J. Dong, J.-Y. You, B. Gu, and G. Su, Strain-Induced Room-Temperature Ferromagnetic Semiconductors with Large Anomalous Hall Conductivity in Two-Dimensional $Cr_2Ge_2Se_6$, Phys. Rev. Appl. **12**, 014020 (2019).

[15] Y. Ren, Y. Ge, W. Wan, Q. Li, and Y. Liu, Two dimensional ferromagnetic semiconductor: Monolayer $CrGeS_3$, J. Phys.: Condens. Matter **32**, 015701 (2020).

[16] J.-Y. You, Z. Zhang, X.-J. Dong, B. Gu, and G. Su, Two-dimensional magnetic semiconductors with room Curie temperatures, Phys. Rev. Res. **2**, 013002 (2020).

[17] A. Kabiraj, M. Kumar, and S. Mahapatra, High-throughput discovery of high Curie point two-dimensional ferromagnetic materials, npj Comput. Mater. **6**, 35 (2020).

[18] C. Gong and X. Zhang, Two-dimensional magnetic crystals and emergent heterostructure devices, Science **363**, eaav4450 (2019).

[19] J. Lee, T. Y. Ko, J. H. Kim, H. Bark, B. Kang, S.-G. Jung, T. Park, Z. Lee, S. Ryu, and C. Lee, Structural and optical properties of single- and few-layer magnetic semiconductor $CrPS_4$, ACS Nano **11**, 10935 (2017).

[20] J. Son, S. Son, P. Park, M. Kim, Z. Tao, J. Oh, T. Lee, S. Lee, J. Kim, K. Zhang, K. Cho, T. Kamiyama, J. H. Lee, K. F. Mak, J. Shan, M. Kim, J.-G. Park, and J. Lee, Air-stable and layer-dependent ferromagnetism in atomically thin van der Waals $CrPS_4$, ACS Nano **15**, 16904 (2021).

[21] Q. L. Pei, X. Luo, G. T. Lin, J. Y. Song, L. Hu, Y. M. Zou, L. Yu, W. Tong, W. H. Song, W. J. Lu, and Y. P. Sun, Spin dynamics, electronic and thermal transport properties of two-dimensional $CrPS_4$ single crystal, J. Appl. Phys. **119**, 043902 (2016).

[22] H. L. Zhuang and J. Zhou, Density functional theory study of bulk and single-layer magnetic semiconductor $CrPS_4$, Phys. Rev. B **94**, 195307 (2016).

[23] M. Joe, H. Lee, M. M. Alyörük, J. Lee, S. Y. Kim, C. Lee, and J. H. Lee, A comprehensive study of piezomagnetic response in $CrPS_4$ monolayer: Mechanical, electronic properties and magnetic ordering under strains, J. Phys.: Condens. Matter **29**, 405801 (2017).

[24] S. Calder, A. V. Haglund, Y. Liu, D. M. Pajerowski, H. B. Cao, T. J. Williams, V. O. Garlea, and D. Mandrus, Magnetic structure and exchange interactions in the layered semiconductor $CrPS_4$, Phys. Rev. B **102**, 024408 (2020).

[25] Y. Peng, S. Ding, M. Cheng, Q. Hu, J. Yang, F. Wang, M. Xue, Z. Liu, Z. Lin, M. Avdeev, Y. Hou, W. Yang, Y. Zheng, and J. Yang, Magnetic structure and metamagnetic transitions in the van der Waals antiferromagnet $CrPS_4$, Adv. Mater. **32**, 2001200 (2020).

[26] R. Diehl and C. D. Carpentier, The crystal structure of chromium thiophosphate, $CrPS_4$, Acta Cryst. B **33**, 1399 (1977).

[27] A. Louisy, G. Ouvrard, D. M. Schleich, and R. Brec, Physical properties and lithium intercalates of $CrPS_4$, Solid State Commun. **28**, 61 (1978).

[28] J. Deng, J. Guo, H. Hosono, T. Ying, and X. Chen, Two-dimensional bipolar ferromagnetic semiconductors from layered antiferromagnets, Phys. Rev. Mater. **5**, 034005 (2021).

[29] A. I. Liechtenstein, M. I. Katsnelson, V. P. Antropov, and V. A. Gubanov, Local spin density functional approach to the theory of exchange interactions in ferromagnetic metals and alloys, J. Magn. Magn. Mater. **67**, 65 (1987).

[30] X. Wan, Q. Yin, and S. Y. Savrasov, Calculation of Magnetic Exchange Interactions in Mott-Hubbard Systems, Phys. Rev. Lett. **97**, 266403 (2006).

[31] P. Blaha, K. Schwarz, G. K. Madsen, D. Kvasnicka, and J. Luitz, WIEN2k, *An Augmented Plane Wave+ Local Orbitals Program for Calculating Crystal Properties* (Technische Universität Wien, Vienna, 2001).

[32] J. Klimeš, D. R. Bowler, and A. Michaelides, Chemical accuracy for the van der Waals density functional, J. Phys.: Condens. Matter **22**, 022201 (2010).

[33] J. Klimeš, D. R. Bowler, and A. Michaelides, Van der Waals density functionals applied to solids, Phys. Rev. B **83**, 195131 (2011).

[34] A. Togo and I. Tanaka, First principles phonon calculations in materials science, Scr. Mater. **108**, 1 (2015).

[35] V. I. Anisimov, F. Aryasetiawan, and A. I. Lichtenstein, First-principles calculations of the electronic structure and spectra of strongly correlated systems: The LDA+U method, J. Phys.: Condens. Matter **9**, 767 (1997).

[36] V. V. Mazurenko and V. I. Anisimov, Weak ferromagnetism in antiferromagnets: α-Fe_2O_3 and La_2CuO_4, Phys. Rev. B **71**, 184434 (2005).

[37] X. Wan, T. A. Maier, and S. Y. Savrasov, Calculated magnetic exchange interactions in high-temperature superconductors, Phys. Rev. B **79**, 155114 (2009).

[38] M. I. Katsnelson, Y. O. Kvashnin, V. V. Mazurenko, and A. I. Lichtenstein, Correlated band theory of spin and orbital contributions to Dzyaloshinskii-Moriya interactions, Phys. Rev. B **82**, 100403(R) (2010).

[39] X. Wan, J. Dong, and S. Y. Savrasov, Mechanism of magnetic exchange interactions in europium monochalcogenides, Phys. Rev. B **83**, 205201 (2011).

[40] D. Wang, X. Bo, F. Tang, and X. Wan, Calculated magnetic exchange interactions in the Dirac magnon material Cu_3TeO_6, Phys. Rev. B **99**, 035160 (2019).

[41] X. Bo, D. Wang, B. Wan, and X. G. Wan, Calculated magnetic exchange interactions in the quantum spin chain materials $K_2CuSO_4Cl_2$ and $K_2CuSO_4Br_2$, Phys. Rev. B **101**, 024416 (2020).

[42] X. Bo, D. Wang, and X. Wan, Calculated magnetic exchange interactions in brownmillerite $Ca_2Fe_2O_5$, Phys. Lett. A **394**, 127202 (2021).

[43] Z.-X. Shen, X. Bo, K. Cao, X. Wan, and L. He, Magnetic ground state and electron-doping tuning of Curie temperature in Fe_3GeTe_2: First-principles studies, Phys. Rev. B **103**, 085102 (2021).

[44] X. Bo, F. Li, X. Xu, X. Wan, and Y. Pu, Calculated magnetic exchange interactions in the van der Waals layered magnet CrSBr, New J. Phys. **25**, 013026 (2023).

[45] K. Cao, G.-C. Guo, D. Vanderbilt, and L. He, First-Principles Modeling of Multiferroic RMn_2O_5, Phys. Rev. Lett. **103**, 257201 (2009).

[46] P. W. Anderson, Antiferromagnetism. Theory of superexchange interaction, Phys. Rev. **79**, 350 (1950).

[47] J. B. Goodenough, An interpretation of the magnetic properties of the perovskite-type mixed crystals $La_{1-x}Sr_xCoO_{3-\lambda}$, J. Phys. Chem. Solids **6**, 287 (1958).

[48] J. Kanamori, Superexchange interaction and symmetry properties of electron orbitals, J. Phys. Chem. Solids **10**, 87 (1959).

[49] C. C. Mayorga-Martinez, Z. Sofer, D. Sedmidubský, Š. Huber, A. Y. S. Eng, and M. Pumera, Layered metal thiophosphite materials: Magnetic, electrochemical, and electronic properties, ACS Appl. Mater. Interfaces **9**, 12563 (2017).